Results in Applied Mathematics 21 (2024) 100420

Contents lists available at ScienceDirect

Results in Applied Mathematics

journal homepage: www.elsevier.com/locate/results-in-applied-mathematics

Numerical modelling of advection diffusion equation using Chebyshev spectral collocation method and Laplace transform

Farman Ali Shah [a], Kamran [a,*], Kamal Shah [b,c], Thabet Abdeljawad [b,**]

[a] Department of Mathematics, Islamia College Peshawar, Peshawar 25120, Khyber Pakhtunkhwa, Pakistan
[b] Department of Mathematics and Sciences, Prince Sultan University, Riyadh 11586, Saudi Arabia
[c] Department of Mathematics, University of Malakand, Chakdara, Dir(L), KPK, Pakistan

ARTICLE INFO

Keywords:
Laplace transform
Numerical inverse Laplace transform
Advection diffusion problems
Spectral collocation method
Contour integration method
Trapezoidal rule

ABSTRACT

In this article a numerical method for numerical modelling of advection diffusion equation is developed. The proposed method is based on Laplace transform (LT) and Chebyshev spectral collocation method (CSCM). The LT is used for time-discretization and the CSCM is used for discretization of spatial derivatives. The LT is used to transform the time variable and avoid the finite difference time stepping method. In time stepping technique the accuracy is achieved for very small time step which results in a very high computational time. The spatial operators are discretized using CSCM to achieve high accuracy as compared to other methods. The method is composed of three primary stages: firstly the given problem is transformed into a corresponding inhomogeneous elliptic problem by using the LT; secondly the CSCM used to solve the transformed problem in LT domain; finally the solution obtained in LT domain is converted to time domain via numerical inverse LT. The inversion of LT is generally an ill-posed problem and due to this reason various numerical inversion methods have been developed. In this article we have utilized the contour integration method which is one of the most efficient methods. The most important feature of this approach is that it handles the time derivative with the Laplace transform rather than the finite difference time stepping approach, avoiding the untoward impact of time steps on stability and accuracy of the method. Five test problems are used to validate the efficiency and accuracy of the proposed numerical scheme.

1. Introduction

A highly current problem is the diffusion behaviour of particles moving in complicated heterogeneous environments. Diffusion is the overall movement of anything from a location of higher concentration to a region of lower concentration. Both abiotic and biotic systems frequently experience the diffusion phenomena [1]. Diffusion is a stochastic process that can be utilized to model a variety of stochastic situations that occur in real life. It plays important role in many disciplines such as physics, including statistics, probability theory, information theory, neural networks, finance, marketing, etc [2–6].

Advection diffusion equation (ADE) is an important equation in the family of diffusion equations which plays important role in many physical systems such as mass and heat transfer, energy, fluid flow, vorticity, etc [7]. This equation can describe physical phenomena where energy is transformed due to two processes advection and diffusion [8]. ADE can also be used to describe water transfer in soils [9], transport of pollutants in the atmosphere [10], volumetric concentration of a pollutant [11], etc.

* Corresponding author.
** Corresponding author.
E-mail addresses: kamran.maths@icp.edu.pk (Kamran), tabdeljawad@psu.edu.sa (T. Abdeljawad).

https://doi.org/10.1016/j.rinam.2023.100420
Received 4 September 2023; Received in revised form 28 October 2023; Accepted 3 December 2023
Available online 8 December 2023

Many analytical methods have been devised for the treatment of ADEs. The analytical solution of a 1-D ADE with variable coefficients on a finite domain has been investigated by Kumar [12]. Kumar and Jaiswal [13] studied the solution of ADE on semi-infinite domain. The authors of [14] examined the analytic solution of ADE. The analytical solution of 2-D ADEs occurring in the distribution of cytosolic calcium concentration was investigated in [15]. In [16], the author obtained semi analytic solution of ADE for modelling solute transport in layered porous media using LT. In [17], the authors derived some the stability results for finite difference method corresponding to linear ADEs. However, the analytical solution for ADEs is not always available. Hence, numerical methods are then employed to get at the desired solution.

The authors of [18] obtained the solution of 1-D ADE using restrictive Taylor's method. Thongmoon [19] compared different numerical methods for the solution of ADE. Chen and Hon [20] obtained the solution of the 2-D and 3-D Helmholtz and convection–diffusion equation using boundary knot method. The authors of [21] examined the solution of ADE using meshless local Petro-Galerkin method. Manohar and Stephenson [22] obtained the solution of ADE via a novel finite difference method. In [23] the authors obtained the numerical solution of 1-D ADE using local RBF method coupled with LT. The authors have used three different numerical techniques for the inversion of LT. Kamran et al. [24] studied the numerical solution ADEs with fractional order derivative using a local RBF method coupled with Laplace transform, the inverse of LT is obtained using contour integration method. Nazir et al. [25] utilized cubic trigonometric B-splines to investigate the solution of ADE.

Spectral methods are among the most popular methods that can solve the numerous partial differential equations (PDEs) more accurately and efficiently [26]. Spectral methods are global, fast and more accurate for sufficiently regular geometries as compared to other numerical methods. Because they are more accurate than the finite difference and finite element approaches, spectral methods have been employed widely in recent years for the numerical solution of PDEs. Due to high accuracy and efficiency spectral techniques have been used by many authors. For example, the method for numerical integration using spectral collocation method was examined by Clenshaw [27]. Gottlieb [28] investigated the problems in fluid dynamics and meteorology via spectral method. A modified Chebyshev pseudo-spectral method with a time step restriction was proposed by Koslo in [29]. The book [30] cover an extensive list of applications as well as the fundamentals of spectral collocation methods. Carpenter [31] emphasized the potential benefits of spectrum approaches that are not restricted to certain quadrature points. The specific applications in their work, however, employed arbitrary grids that were not connected to any orthogonal basis set. Weideman [32] revealed some preliminary calculations made with unconventional basis sets. Mofid [33] discussed the Stability of the Chebyshev collocation approximation to the ADE. Elghaoui [34] examined the spectral embedding method applied to the ADE. Reddy [35] elaborated the Pseudospectra and the ADE operator. Gottlieb [36] discussed the spectrum of the Chebyshev collocation operator for the heat equation. Orovio [37] discussed the spectral Methods for PDEs in complex domains. However, the finite difference methodology is used in all of the aforementioned methods to discretize time. With these techniques, accuracy can be obtained in extremely short time steps. These methods also have crucial stability constraints. The alternate solution is to apply the Laplace transform (LT) in order to avoid these problems [38].

In order to numerically simulate ADE, the LT and Chebyshev spectral collocation method (CSCM) are coupled in this paper. This paper is first attempt to utilize the LT coupled with CSCM. The LT is an effective tool that is frequently utilized in literature along with other PDE modelling techniques. It has been proven that the LT is suitable for solving various initial and boundary value problems and can be utilized as an alternative to the time stepping technique [39]. However, the fundamental challenge with the LT is its inversion. Numerous algorithms for the inversion of LT are available such as the Crump method [40], the De Hoog method [41], the Weeks method [42,43], etc. However, in this work we have utilized the contour integration method proposed in [44] for numerical inverse LT. We consider a two dimensional ADE in a domain Φ with boundary $\partial\Phi$ of the form

$$\begin{aligned} D_t\mathcal{U}(\boldsymbol{\sigma},t) &= \zeta\Delta\mathcal{U}(\boldsymbol{\sigma},t) + \xi\nabla\mathcal{U}(\boldsymbol{\sigma},t) - \lambda\mathcal{U}(\boldsymbol{\sigma},t) + Q(\boldsymbol{\sigma},t), \\ &= \mathcal{L}\mathcal{U}(\boldsymbol{\sigma},t) + Q(\boldsymbol{\sigma},t), \ \boldsymbol{\sigma}\in\Phi, \quad t\in[0,1], \end{aligned} \tag{1}$$

with BCs

$$\mathcal{U}(\boldsymbol{\sigma},t) = h(\boldsymbol{\sigma},t), \ \boldsymbol{\sigma}\in\partial\Phi, \quad t\in[0,1], \tag{2}$$

and ICs

$$\mathcal{U}(\boldsymbol{\sigma},0) = \mathcal{U}_0(\boldsymbol{\sigma}), \ \boldsymbol{\sigma}\in\Phi, \tag{3}$$

where $\mathcal{L}\mathcal{U}(\boldsymbol{\sigma},t) = \zeta\Delta\mathcal{U}(\boldsymbol{\sigma},t) + \xi\nabla\mathcal{U}(\boldsymbol{\sigma},t) - \lambda\mathcal{U}(\boldsymbol{\sigma},t)$, $D_t = \frac{\partial}{\partial t}$, $Q(\boldsymbol{\sigma},t)$, $\mathcal{U}_0(\boldsymbol{\sigma})$, $h(\boldsymbol{\sigma},t)$ are given continuous functions, ζ,ξ, and λ are arbitrary coefficients, and $\Phi\subset\mathbb{R}^2$ is a bounded domain with boundary $\partial\Phi$.

2. Existence and uniqueness of solution

The following hypothesis will be needed for the uniqueness and existence results of problem defined in (1)–(3).
Consider Eq. (1)–(3) as

$$\begin{cases} D_t\mathcal{U}(\boldsymbol{\sigma},t) = f(\mathcal{U}(\boldsymbol{\sigma},t),t), \quad t\in[0,1], \\ \mathcal{U}(\boldsymbol{\sigma},0) = \mathcal{U}_0(\boldsymbol{\sigma}), \quad \boldsymbol{\sigma}\in\Phi. \end{cases} \tag{4}$$

For the function $f(\mathcal{U}(\boldsymbol{\sigma},t),t)$ the following condition holds:
A_1 : for any $g:[0,1]\to\mathbb{R}^+$, $\mathcal{U}$ *and* $\overline{\mathcal{U}}$ be two solutions, then

$$|f(\mathcal{U}(\boldsymbol{\sigma},t),t) - f(\overline{\mathcal{U}}(\boldsymbol{\sigma},t),t)| \le g(t)|\mathcal{U}(\boldsymbol{\sigma},t) - \overline{\mathcal{U}}(\boldsymbol{\sigma},t)|,$$

and

$$\max_{t\in[0,1]}\int_0^t |g(s)|ds = L.$$

Theorem 1. *In view of* (A_1) *and if the assumption and the condition*

$$\max_{t\in[0,1]}\int_0^t |g(s)|ds = L < 1,$$

hold, then the problem (4) *has a unique solution by using the Banach contraction theorem.*

Proof. The equivalent integral form of Eq. (4) is given by

$$\mathcal{U}(\boldsymbol{\sigma},t) = \mathcal{U}_0(\boldsymbol{\sigma}) + \int_0^t f(\mathcal{U}(\boldsymbol{\sigma},s),s)ds,\ \ \boldsymbol{\sigma}\in\boldsymbol{\Phi}.$$

Let us define a Banach space $\mathcal{B} = [0,1]\times\boldsymbol{\Phi}$, such that

$$\|\mathcal{U}\| = \sup_{t\in[0,1]} |\mathcal{U}(\boldsymbol{\sigma},t)|.$$

Then, we define an operator $N : \mathcal{B} \to \mathcal{B}$ by

$$N(\mathcal{U}(\boldsymbol{\sigma},t)) = \mathcal{U}_0(\boldsymbol{\sigma}) + \int_0^t f(\mathcal{U}(\boldsymbol{\sigma},s),s)ds,\ \ \boldsymbol{\sigma}\in\boldsymbol{\Phi}. \tag{5}$$

Form Eq. (5), we have for any $\mathcal{U}, \overline{\mathcal{U}} \in \mathcal{B}$, such that

$$\begin{aligned}
\|N\mathcal{U} - N\overline{\mathcal{U}}\| &= \max_{\substack{t\in[0,1]\\ \boldsymbol{\sigma}\in\boldsymbol{\Phi}}} |N\mathcal{U}(\boldsymbol{\sigma},t) - N\overline{\mathcal{U}}(\boldsymbol{\sigma},t)|,\\
&= \max_{\substack{t\in[0,1]\\ \boldsymbol{\sigma}\in\boldsymbol{\Phi}}} |\int_0^t \left[f(\mathcal{U}(\boldsymbol{\sigma},s),s) - f(\overline{\mathcal{U}}(\boldsymbol{\sigma},s),s)\right]ds|,\\
&\le \max_{\substack{t\in[0,1]\\ \boldsymbol{\sigma}\in\boldsymbol{\Phi}}} \int_0^t |f(\mathcal{U}(\boldsymbol{\sigma},s),s) - f(\overline{\mathcal{U}}(\boldsymbol{\sigma},s),s)|ds,\\
&\le \max_{\substack{t\in[0,1]\\ \boldsymbol{\sigma}\in\boldsymbol{\Phi}}} \int_0^t |g(s)||\mathcal{U}(\boldsymbol{\sigma},s) - \overline{\mathcal{U}}(\boldsymbol{\sigma},s)|ds,\\
&\le \|\mathcal{U} - \overline{\mathcal{U}}\| \max_{t\in[0,1]} \int_0^t |g(s)|ds.
\end{aligned}$$

Then we have

$$\|N\mathcal{U} - N\overline{\mathcal{U}}\| \le L\|\mathcal{U} - \overline{\mathcal{U}}\|.$$

Hence N is a contraction. Hence Eq. (4) has a unique solution.

3. Numerical scheme

In our proposed methodology first the LT is employed to the model defined in (1)–(3) and reduce it an elliptic problem in LT domain. Secondly, we employ the CSCM to approximate the solution of the transformed problem in LT. Finally, the LT is numerically inverted in order to recover the original problem's solution.

3.1. (i) Time discretization

In this section we employ the LT for time discretization. The given 2D ADE is transformed via LT to a time independent problem. Let $\mathcal{U}(\boldsymbol{\sigma},t)$ be a piecewise continuous function defined for $t > 0$, and let $\widehat{\mathcal{U}}(\boldsymbol{\sigma},z)$ be its LT given as

$$\widehat{\mathcal{U}}(\boldsymbol{\sigma},z) = \int_0^\infty exp(-zt)\mathcal{U}(\boldsymbol{\sigma},t)dt.$$

The LT of $D_t\mathcal{U}(\boldsymbol{\sigma},t)$ has the following form

$$\mathscr{L}\left[D_t\mathcal{U}(\boldsymbol{\sigma},t)\right] = z\widehat{\mathcal{U}}(\boldsymbol{\sigma},z) - \mathcal{U}_0.$$

Applying the LT to (1)–(3), we get

$$z\widehat{\mathcal{U}}(\boldsymbol{\sigma},z) - \mathcal{U}_0 - \mathcal{L}\widehat{\mathcal{U}}(\boldsymbol{\sigma},z) = \widehat{Q}(\boldsymbol{\sigma},t), \tag{6}$$

and

$$\widehat{U}(\sigma, z) = \hat{h}(\sigma, z). \tag{7}$$

Simplifying (6)–(7) we get

$$(zI - \mathcal{L})\widehat{U}(\sigma, z) = \widehat{G_1}(\sigma, z), \tag{8}$$

$$\widehat{U}(\sigma, z) = \hat{h}(\sigma, z), \tag{9}$$

where,

$$\widehat{G_1}(\sigma, z) = U_0 + \hat{Q}(\sigma, z),$$

here I is the identity operator. In order to solve the system (8)–(9), first we need to employ the CSCM for the discretization of the operator $\mathcal{L}$. Following that we solve the system in LT domain for each node z along a suitable contour of integration in the LT domain (see, e.g., [45]). Finally, the inverse LT is used to obtain the solution of the problem ((1)–(3)). The next section describe the CSCM in detail.

3.2. (iii) Chebyshev spectral collocation method

CSCM is an efficient and highly accurate method for the numerical approximation of the solution of PDEs. Using CSCM the data $\left\{\left(x_j, \widehat{U}(x_j)\right)\right\}$ is interpolated via the nth degree Lagrange interpolation polynomial (LIP) $\wp_j(x)$ as [30]

$$I_p^m(x) = \sum_{j=0}^{m} \wp_j(x)\widehat{U}(x_j), \tag{10}$$

where $\wp_j(x)$ at the points $\{x_j\}_{j=0}^m$ are given as

$$\wp_j(x) = \prod_{i=0,\ i\neq j}^{n} \frac{(x - x_i)}{(x_j - x_i)},\ j = 0, 1, 2, 3, \ldots, m, \tag{11}$$

The Chebyshev points defined as

$$x_j = \left\{\cos\left(\frac{j\pi}{m}\right)\right\}_{j=0}^{m}, \tag{12}$$

are used to discretize the domain $[-1, 1]$. The first derivative $\frac{\partial \widehat{U}}{\partial x}$ can be approximated using Chebyshev nodes as

$$\frac{\partial \widehat{U}}{\partial x} \approx \mathcal{D}_m \widehat{U}, \tag{13}$$

the entries of $\mathcal{D}_m$ are given as

$$[\mathcal{D}_m]_{i,j} = \wp_j'(x_i),\ i, j = 1, 2, 3, \ldots, m,$$

and the off-diagonal elements of $[\mathcal{D}_m]_{i,j}$ have the following form

$$[\mathcal{D}_m]_{i,j} = \frac{\alpha_j}{\alpha_i(x_i - x_j)},\ i \neq j, \tag{14}$$

where $\alpha_j^{-1} = \prod_{i\neq j}^{m}(x_i - x_j)$, and the diagonal elements are

$$[\mathcal{D}_m]_{i,j} = -\sum_{j=0,\ j\neq i}^{m} [\mathcal{D}_m]_{i,j},\ i = 0, 1, 2, 3, \ldots, m.$$

Next, we can analytically obtained the entries of υth-order matrix $\mathcal{D}_m^{\upsilon}$ as

$$[\mathcal{D}_m^{\upsilon}]_{i,j} = \wp_j^{\mu}(x_i),\ i, j = 1, 2, \ldots, m. \tag{15}$$

For more stable and efficient computation the readers are referred to [46,47] . The authors of [47] obtained an applicable formula for obtaining derivatives of interpolation matrices as

$$[\mathcal{D}_m^{\upsilon}]_{ij} = \frac{\upsilon}{x_i - x_j}\left(\frac{\alpha_j}{\alpha_i}[\mathcal{D}_m^{(\upsilon-1)}]_{ii} - [\mathcal{D}_m^{(\upsilon-1)}]_{ij}\right),\ i \neq j.$$

the points σ_{ij} in 2D are expressed as

$$\sigma_{ij} = \left(\cos\left(\frac{i\pi}{m}\right), \cos\left(\frac{j\pi}{m}\right)\right),\ i, j = 0, 1, 2, 3, \ldots, m,$$

and the LIP are expressed as

$$\wp_{ij}(\boldsymbol{\sigma}) = \wp_i(x)\wp_j(y),\ \ i,j = 0,1,2,\dots,m, \tag{16}$$

where $\wp_{ij}(\boldsymbol{\sigma}_{ij}) = \delta_{ij}$, the 2^{nd}-order derivatives of the LIPs (16) are obtained as

$$\frac{\partial^2 \wp_{ij}(\boldsymbol{\sigma}_{rs})}{\partial x^2} = \wp_i''(x_r)\wp_j(y_s) = [\boldsymbol{D}_{\boldsymbol{n}}^2]_{ri}\delta_{js},$$

$$\frac{\partial^2 \wp_{ij}(\boldsymbol{\sigma}_{rs})}{\partial y^2} = \wp_i(x_r)\wp_j''(y_s) = \delta_{ri}[\boldsymbol{D}_{\boldsymbol{n}}^2]_{sj},$$

where $\boldsymbol{D}_m^2$ is 2^{nd}-order matrix. $\mathcal{L}$ is applied on the LIPs at the nodes $\{\boldsymbol{\sigma}_{rs}\}$ as

$$\mathcal{L}(\wp_{ij}(\boldsymbol{\sigma}_{rs})) = \zeta\left([\boldsymbol{D}_m^2]_{ri}\delta_{js} + \delta_{ri}[\boldsymbol{D}_m^2]_{sj}\right) + \xi\left([\boldsymbol{D}_m]_{ri}\delta_{js} + \delta_{ri}[\boldsymbol{D}_m]_{sj}\right) - \lambda\delta_{ri}\delta_{sj}. \tag{17}$$

It is possible to write the linear operator (17) in a matrix form as

$$\boldsymbol{\mathcal{L}}_{Disc} = \zeta\left(I_m \otimes \boldsymbol{D}_m^2 + \boldsymbol{D}_m^2 \otimes I_m\right) + \xi\left(I_m \otimes \boldsymbol{D}_m + \boldsymbol{D}_m \otimes I_m\right) - \lambda\left(I_m \otimes I_m\right). \tag{18}$$

Now using the differentiation matrix $\boldsymbol{\mathcal{L}}_{Disc}$ in Eq. (8), we have

$$(zI - \boldsymbol{\mathcal{L}}_{Disc})\widehat{\mathcal{U}}(\boldsymbol{\sigma}, z) = \widehat{G_1}(\boldsymbol{\sigma}, z). \tag{19}$$

The boundary conditions in (9) can be incorporated by considering the matrix $\boldsymbol{\mathcal{L}}_{Disc}$ on all points $\boldsymbol{\sigma}$ and the rows of $\boldsymbol{\mathcal{L}}_{Disc}$ corresponding to boundary points are replaced with unit vectors having a one corresponding to the diagonal of $\boldsymbol{\mathcal{L}}_{Disc}$. Hence, the boundary conditions $\mathcal{U}(\boldsymbol{\sigma}, t) = h(\boldsymbol{\sigma}, t)$ will be enforced explicitly [30]. Finally, the approximate solution $\widehat{\mathcal{U}}(\boldsymbol{\sigma}, z)$ is obtained in LT domain by Eq. (8) is solved for each node z. Then the solution $\widehat{\mathcal{U}}(\boldsymbol{\sigma}, t)$ of the problem Eq.(1)– (3) is obtained via inverse LT.

3.2.1. Stability of the numerical scheme

For the nodes given in Eq. (12) and the LIPs in Eq. (11), the interpolation operator can be expressed as:

$$\boldsymbol{I}_p^m : C(\boldsymbol{\Phi}) \to \mathcal{P}_m, \quad \boldsymbol{I}_p^m(\mathcal{U}) = \sum_{j=0}^{m} \mathcal{U}(x_j)\wp_j(x). \tag{20}$$

Borm et al. [48] proposed the basic steps for the constructing the stability bound. For a constant M_m, we have the following stability estimate

$$\|\boldsymbol{I}_p^m(\mathcal{U})\|_\infty \le M_m\|\mathcal{U}\|_\infty, \quad \forall\ \mathcal{U} \in C[-1,1]. \tag{21}$$

Furthermore,

$$\boldsymbol{I}_p^m(\mathcal{U}) = \mathcal{U}, \quad \forall \quad \mathcal{U} \in \mathcal{P}_m. \tag{22}$$

For Chebyshev interpolation we have

$$M_m = \frac{2ln(1+m)}{\pi} + 1 \le (1+m). \tag{23}$$

This shows that the constant of stability depends on m and develops very slowly. Also, for $\mathcal{U} \in C^{m+1}[-1,1]$, the following bound [48] holds:

$$\|\mathcal{U} - \boldsymbol{I}_p^m(\mathcal{U})\|_\infty \le \frac{1}{2^m\Gamma(m+2)}\|\mathcal{U}^{(m+1)}\|_\infty. \tag{24}$$

Theorem 2 (*[48]*). *If (21) and (24) hold, for $\mathcal{U} \in C^{(m+1)}[-1,1]$, then we have*

$$\|\mathcal{U}^{(k)} - \boldsymbol{I}_p^m(\mathcal{U})^{(k)}\|_\infty \le \frac{2^k(M_m^{(k)}+1)}{2^m\Gamma(m-k+2)}\|\mathcal{U}^{(m+1)}\|_\infty,\ \ k = 1,2,3,\dots,m, \tag{25}$$

which depends on the following stability constant

$$M_m^{(k)} = \frac{M_m}{\Gamma(k+1)}\left(\frac{\Gamma(m+1)}{\Gamma(m-k+1)}\right). \tag{26}$$

Proof. Now, using the (24)–(25) for the ADE (1) in 1-D, the error estimate is given as

$$\begin{aligned}
\mathbb{E} &= \|(D_t\mathcal{U} - \mathcal{L}\mathcal{U}) - (D_t \boldsymbol{I}_p^m(\mathcal{U}) - \mathcal{L}\boldsymbol{I}_p^m(\mathcal{U}))\|_\infty,\\
&= \|(D_t(\mathcal{U} - \boldsymbol{I}_p^m(\mathcal{U}))) - \mathcal{L}(\mathcal{U} - \boldsymbol{I}_p^m(\mathcal{U}))\|_\infty,\\
&\le \|(D_t(\mathcal{U} - \boldsymbol{I}_p^m(\mathcal{U})))\|_\infty + \|\mathcal{L}(\mathcal{U} - \boldsymbol{I}_p^m(\mathcal{U}))\|_\infty,\\
&\le \|D_t(\mathcal{U} - \boldsymbol{I}_p^m(\mathcal{U}))\|_\infty + |\zeta|\|\mathcal{U}_{xx} - \boldsymbol{I}_p^m(\mathcal{U})_{xx}\|_\infty\\
&+ |\xi|\|\mathcal{U}_x - \boldsymbol{I}_p^m(\mathcal{U})_x\|_\infty + |\lambda|\|\mathcal{U} - \boldsymbol{I}_p^m(\mathcal{U})\|_\infty,\\
\mathbb{E} &\le \|D_t(\mathcal{U} - \boldsymbol{I}_p^m(\mathcal{U}))\|_\infty + |\zeta|\frac{2^2(M_m^{(2)}+1)}{2^m\Gamma(m)}\|\mathcal{U}^{(m+1)}\|_\infty\\
&+ |\xi|\frac{2(M_m^{(1)}+1)}{2^m\Gamma(1+m)}\|\mathcal{U}^{(m+1)}\|_\infty + |\lambda|\frac{1}{2^m\Gamma(m+2)}\|\mathcal{U}^{(m+1)}\|_\infty,
\end{aligned} \tag{27}$$

since the time derivative can be evaluated accurately, so the error bound of $\|D_t(\mathcal{U} - \boldsymbol{I}_p^m(\mathcal{U}))\|_\infty$ and $\|\mathcal{U} - \boldsymbol{I}_p^m(\mathcal{U})\|_\infty$ are the same, so we have

$$\mathbb{E} \le \mathcal{M}\|\mathcal{U}^{(m+1)}\|_\infty. \tag{28}$$

where $\mathcal{M}$ is the sum of coefficients of $\|\mathcal{U}^{(m+1)}\|_\infty$. To prove similar stability results for 2D problems, the tensor product interpolation operators can be used.

3.3. (iv) Inverse Laplace transform

The numerical inverse LT techniques are discussed in this section. The contour integration approach is employed for inverting the LT numerically. In the mentioned approach the solution $\mathcal{U}(\boldsymbol{\sigma}, t)$ is written as

$$\mathcal{U}(\boldsymbol{\sigma}, t) = \frac{1}{2\pi i}\int_{\varrho - i\infty}^{\varrho + i\infty} e^{zt}\widehat{\mathcal{U}}(\boldsymbol{\sigma}, z)dz = \frac{1}{2\pi i}\int_{\Gamma} e^{zt}\widehat{\mathcal{U}}(\boldsymbol{\sigma}, z)dz,\ t > 0,\ \varrho > \varrho_0, \tag{29}$$

where Γ is properly chosen integration contour in the complex plane connecting $\varrho - i\infty$ to $\varrho + i\infty$. The integral defined in (29) is known as Bromwich integral. Solution of (1)–(3) depends on the computation of the Bromwich integral along a suitable contour Γ in the complex plane. For complicated function the analytic evaluation of this integral becomes very tedious. Therefore, various numerical techniques are devised in literature for the numerical computation of the Bromwich integral. Because of the highly oscillatory exponential factor e^{zt} on the contour Γ and the slowly decaying transform function $\widehat{\mathcal{U}}(\boldsymbol{\sigma}, z)$, $z = \varrho + iy$, as $y \to \infty$numerical integration of the integral defined by Eq. (29) is difficult to perform. To handle the difficulty of the slow decay of the transform function $\widehat{\mathcal{U}}(\boldsymbol{\sigma}, z)$ the idea of Talbot [49] can be utilized. According to Talbots suggestion the Bromwich line $z = \varrho + iy,\ -\infty < y < \infty$ may be changed to a contour that starts and ends in the left half plane, so that the integrand in Eq. (29) decays fast due to the exponential factor. As a result, the integral described by Eq. (29) is appropriate to approximation using the mid point or trapezoidal rule [50]. According to Cauchy's theorem, such a deformation is permitted if $\widehat{\mathcal{U}}(\boldsymbol{\sigma}, z)$ has no singularities and $|\widehat{\mathcal{U}}(\boldsymbol{\sigma}, z)| \to 0$ if $Re(z) \le \varrho_0$ as $|z| \to \infty$. (If $\mathcal{U}(\boldsymbol{\sigma}, z)$ contains singularities with an unbounded imaginary portion, the Talbot approach may fail).

An ideal contour that is parabolic or hyperbolic can be used to solve Eq. (29) as efficiently as possible. For the numerical approximation of the inverse Laplace transform, many contour integration techniques are developed [44,51]. In this work, the hyperbolic contour in [44] is utilized, which is given in parametric form as

$$z(\eta) = \omega + \lambda(1 - sin(\delta - i\eta)), \text{for } \eta \in \mathbb{R}, \tag{30}$$

with $\lambda > 0$, $\omega \ge 0$, $0 < \delta < \beta - \frac{1}{2}\pi$, and $\frac{1}{2}\pi < \beta \le \bar{\beta} < \pi$ (for detail see [44]). Using Eq. (30) in Eq. (29), we get

$$\mathcal{U}(\boldsymbol{\sigma}, t) = \frac{1}{2\pi i}\int_{\Gamma} e^{-zt}\widehat{\mathcal{U}}(\boldsymbol{\sigma}, z)dz = \frac{1}{2\pi i}\int_{-\infty}^{\infty} e^{-z(\eta)t}\widehat{\mathcal{U}}(\boldsymbol{\sigma}, (z(\eta)))z'(\eta)d\eta, \tag{31}$$

The integral defined (31) can be approximated via the trapezoidal rule with step k as

$$\mathcal{U}_k(\boldsymbol{\sigma}, t) = \frac{k}{2\pi i}\sum_{j=-M}^{M} e^{(z_j)t}\widehat{\mathcal{U}}(\boldsymbol{\sigma}, (z_j)z_j'),\quad z_j = z(\eta_j),\ \eta_j = jk. \tag{32}$$

4. Error analysis

The error analysis of the proposed scheme is discussed in this section. In our scheme first step we employ the Laplace transform and this step is free of error. In the second step we employ the Chebyshev spectral collocation method for the approximation of the solution of the transformed problem. The error of CSCM depends on the theorem stated as

Theorem 3 (*[30], Theorem 5*). *For a given function $\mathcal{U}(\boldsymbol{\sigma}, t)$ and a sequence of sets of interpolation points $\{\boldsymbol{\sigma}_j\}_m$, $m = 1, 2, 3, \ldots$ that converge to a density function ς as $n \to \infty$ with corresponding potential χ given by the integral*

$$\chi(\alpha) = \int_{-1}^{1} \varsigma(v) log|\alpha - v| dv,$$

define $\chi_{[-1,1]} = sup_{v\in[-1,1]}\chi(v)$. *then construct* p_m *of degree* $\leq n$ *for each* n *that interpolates* $\mathcal{U}(\boldsymbol{\sigma},t)$ *at* $\{\boldsymbol{\sigma}_j\}_m$. *If for a constant* $\chi_{\mathcal{U}} > \chi_{[-1,1]}$ *such that* $\mathcal{U}(\boldsymbol{\sigma},t)$ *is analytic through the region*

$$\{\alpha \in \mathbb{C} : \chi(\alpha) \leq \chi_{\mathcal{U}}\},$$

such that there exist a constant $M > 0$ *such that* $\forall \boldsymbol{\sigma} \in [-1,1]$ *and* $\forall n$,

$$|\mathcal{U}(\boldsymbol{\sigma},t) - p_m| \leq M exp^{-m(\chi_{\mathcal{U}} - \chi_{[-1,1]})}.$$

The estimate is still valid, but with a new constant M *for the difference of* μth *derivatives,* $\mathcal{U}^{\mu} - p_n^{\mu}$, $\mu \geq 1$.

In the final step we employ the contour integration technique for the approximating the Bromwich integral defined in. While approximating the integral defined in Eq. (31) the convergence is achieved at different time rates which depends on the contour of integration Γ. The convergence order of the proposed numerical method depends on the quadrature k and the domain $[t_0, T]$. The convergence order of the method is given in the following theorem.

Theorem 4 (*[44], Theorem 2.1*). *Let* $\mathcal{U}(\boldsymbol{\sigma},t)$ *be the solution of Eqs. (1)–(3) with* $\widehat{Q}(s) = \mathscr{L}\{Q(\boldsymbol{\sigma},t)\}$ *be analytic function in the set* Σ_{β}^{ω}. *Let* $0 < t_0 < T$, $0 < \theta < 1$, *and let* $b > 0$ *be defined by* $b = cosh^{-1}\left\{\frac{1}{\theta t \sin(\delta)}\right\}$, *where* $t_1 = \frac{t_0}{T}$. *Let* $0 < r < min(\delta, \beta - \frac{1}{\pi} - \delta)$ *so that* $\Gamma \subset S_r \subset \Sigma_{\beta}^{\omega}$, *and let the scaling factor be* $\lambda = \frac{\theta \bar{r} M}{bT}$. *Then for* $\mathcal{U}_k(\boldsymbol{\sigma},t)$ *defined in Eq. (32), we have* $|\mathcal{U}(\boldsymbol{\sigma},t) - \mathcal{U}_k(\boldsymbol{\sigma},t)| \leq CQe^{\omega t} l(\rho_r M) e^{-\mu_e M}\left(\|\mathcal{U}_0\| + \|\widehat{Q}(s)\|_{\Sigma_{\beta}^{\omega}}\right)$, *with* $\mu_e = \frac{\bar{r}(1-\theta)}{b}$, $k = \frac{b}{M} \leq \frac{\bar{r}}{log2}$, $\rho_r = \frac{\theta \bar{r} t \sin(\delta - r)}{b}$, $\bar{r} = 2\pi r$, $r > 0$, $t_0 \leq t \leq T$, $C = C_{\delta,r,\beta}$, *and* $l(x) = max(1, log(\frac{1}{x}))$. *Hence the estimate is as follows*

$$Est_1 = |\mathcal{U}(\boldsymbol{\sigma},t) - \mathcal{U}_k(\boldsymbol{\sigma},t)| = O(l(\rho_r M)(e^{-\mu_e M})).$$

Theorem 5 (*[44], Theorem 2.2*). *Let* $\mathcal{U}(\boldsymbol{\sigma},t)$ *be the solution of (1), and let* $\widehat{Q}$ *be analytic in the set* $\sum_{\beta}^{\omega}$. *Set* $\gamma = 2\sigma$, $0 < \sigma \leq 1$, *and suppose* $\Gamma \subset S_r \subset \sum_{\beta}^{\omega}$ *is defined as* $\lambda = \frac{\gamma}{\kappa T}$, *with* $\kappa = 1 - sin(\delta - r)$. *Let* $\mathcal{U}_k(\boldsymbol{\sigma},t)$ *be the numerical solution of Eq. (1) with* $k = \sqrt{\frac{\bar{r}}{\gamma M}} \leq \frac{\bar{r}}{log2}$. *Then, if* $\sigma_0, \nu \geq 0$ *and* $\sigma_0 + \frac{1}{2}\nu \geq \sigma$, *we have, with* $C = C_{\delta,r,\beta,\sigma,\sigma_0}$ *for* $0 \leq t \leq T$,

$$\|\mathcal{U}_k(\boldsymbol{\sigma},t) - \mathcal{U}(\boldsymbol{\sigma},t)\| \leq CM\gamma^{-1}T^{\gamma}e^{\omega t}e^{-\sqrt{\bar{r}\gamma N}}\left(\|\mathcal{U}_0\|_{\sigma} + \|\bar{f}\|_{\sigma_0,\nu,\sum_{\beta}^{\omega}}\right).$$

Hence the estimate is as follows

$$Est_2 = |\mathcal{U}(\boldsymbol{\sigma},t) - \mathcal{U}_k(\boldsymbol{\sigma},t)| = O\left(\gamma^{-1}T^{\gamma}e^{\omega t}e^{-\sqrt{\bar{r}\gamma M}}\right).$$

Theorem 6. *Let* $\mathcal{B}$ *is a Banach space such that* $N : \mathcal{B} \to \mathcal{B}$ *is a contraction operator with constant* $0 < L < 1$, *then the series solution produced by inverse Laplace transform method can be expressed as*

$$\mathcal{U}_n = N(\mathcal{U}_{n-1}), \quad \mathcal{U}_{n-1} = \sum_{i=1}^{n-1}\mathcal{U}_i, \ n = 1,2,3,\ldots$$

and

$$\mathcal{U}_n \in S_r(\mathcal{U}) = \left\{\overline{\mathcal{U}} \in \mathcal{B} : \|\mathcal{U} - \overline{\mathcal{U}}\| < r\right\},$$

$$\lim_{n\to\infty}\mathcal{U}_n = \mathcal{U}, \quad where\ \mathcal{U}_0 = \mathcal{U}(\boldsymbol{\sigma},0).$$

Proof. We use mathematical induction here, for $n = 1$, one has

$$\|\mathcal{U}_1 - \mathcal{U}\| = \|N\mathcal{U}_0 - N\mathcal{U}\| \leq L\|\mathcal{U}_0 - \mathcal{U}\|.$$

Let the result is true for $n-1$, then

$$\|\mathcal{U}_{n-1} - \mathcal{U}\| \leq L^{n-1}\|\mathcal{U}_0 - \mathcal{U}\|. \tag{33}$$

Now, we have

$$\|\mathcal{U}_n - \mathcal{U}\| = \|N(\mathcal{U}_{n-1}) - N(\mathcal{U})\| \leq L\|\mathcal{U}_{n-1} - \mathcal{U}\|. \tag{34}$$

By using Eqs. (33) and (34), implies that

$$\|\mathcal{U}_n - \mathcal{U}\| \leq LL^{n-1}\|\mathcal{U}_0 - \mathcal{U}\| \leq L^n.r < r.$$

which yields that

$$\mathcal{U}_n \in S_r(\mathcal{U}). \quad Also\ n \to \infty, \quad L^n \to 0.$$

Table 1
The ϵ_2, ϵ_∞, ϵ_{rms} and Est_1 of the LTCSCM for problem 1.

m	M	ϵ_2	ϵ_∞	ϵ_{rms}	Est_1	C.time (s)
22	90	4.1661×10^{-6}	3.1196×10^{-7}	1.8937×10^{-7}	8.1825×10^{-4}	49.744711
24		4.5150×10^{-6}	3.1196×10^{-7}	1.8812×10^{-7}	8.1825×10^{-4}	75.533196
26		4.8638×10^{-6}	3.1196×10^{-7}	1.8707×10^{-7}	8.1825×10^{-4}	115.754541
28		5.2127×10^{-6}	3.1196×10^{-7}	1.8617×10^{-7}	8.1825×10^{-4}	158.580325
30		5.5615×10^{-6}	3.1196×10^{-7}	1.8538×10^{-7}	8.1825×10^{-4}	217.758343
30	50	5.2457×10^{-3}	2.9431×10^{-4}	1.7486×10^{-4}	6.2465×10^{-2}	67.115453
	60	4.3448×10^{-4}	2.4373×10^{-5}	1.4483×10^{-5}	2.1185×10^{-2}	103.020131
	70	1.3622×10^{-4}	7.6413×10^{-6}	4.5405×10^{-6}	7.1708×10^{-3}	138.346441
	80	1.9642×10^{-5}	1.1018×10^{-6}	6.5473×10^{-7}	2.4236×10^{-3}	180.098122
	90	5.5615×10^{-6}	3.1196×10^{-7}	1.8538×10^{-7}	8.1825×10^{-4}	217.758343

Table 2
The ϵ_2, ϵ_∞, ϵ_{rms} and Est_2 of the LTCSCM for problem 1.

m	M	ϵ_2	ϵ_∞	ϵ_{rms}	Est_2	C.time (s)
22	90	7.6078×10^{-11}	7.7076×10^{-12}	3.4581×10^{-12}	2.2972×10^{-1}	56.417398
24		8.1940×10^{-11}	1.0965×10^{-11}	3.4142×10^{-12}	2.2972×10^{-1}	82.734604
26		9.1547×10^{-11}	1.6342×10^{-11}	3.5210×10^{-12}	2.2972×10^{-1}	138.357102
28		9.6982×10^{-11}	1.6627×10^{-11}	3.4636×10^{-12}	2.2972×10^{-1}	187.622473
30		1.0598×10^{-10}	1.1505×10^{-11}	3.5326×10^{-12}	2.2972×10^{-1}	240.441199
30	50	1.2957×10^{-5}	7.2693×10^{-7}	4.3192×10^{-7}	1.2351×10^{0}	75.537376
	60	3.1824×10^{-8}	1.7859×10^{-9}	1.0608×10^{-9}	7.7317×10^{-1}	110.393963
	70	6.5358×10^{-8}	3.6660×10^{-9}	2.1786×10^{-9}	5.0201×10^{-1}	144.561637
	80	7.3947×10^{-10}	4.9799×10^{-11}	2.4649×10^{-11}	3.3556×10^{-1}	192.887933
	90	1.0598×10^{-10}	1.1505×10^{-11}	3.5326×10^{-12}	2.2972×10^{-1}	240.441199

Therefore

$$\lim_{n\to\infty} \mathcal{U}_n = \mathcal{U}.$$

Which completes the proof.

5. Numerical tests

In this section five test problems are considered to assess the effectiveness and accuracy of the Laplace transformed CSCM. Our numerical results involve the following two sets of parameters for contour integration:

- **Set 1:Theorem 2** $\omega = 0, \theta = 0.1, r = 0.13870, \delta = 0.1541,$ and $t \in [0.5, 5]$
- **Set 2:Theorem 3** $\omega = 1, \sigma = 0.159, r = 0.2551, \gamma = 0.3180,\ \delta = 0.2835,$ and $t \in [0.5, 5]$

We compute the maximum absolute error, the relative error, and the rms error between the numerical and the exact solutions, which are defined as follows:

$$\epsilon_\infty = \max_{1\le j\le m} |\mathcal{U}(\boldsymbol{\sigma}_j, t) - \mathcal{U}_k(\boldsymbol{\sigma}_j, t)|,$$

$$\epsilon_2 = \sqrt{\frac{\sum_{j=1}^{m} (\mathcal{U}(\boldsymbol{\sigma}_j, t) - \mathcal{U}_k(\boldsymbol{\sigma}_j, t))^2}{\sum_{j=1}^{m} (\mathcal{U}(\boldsymbol{\sigma}_j, t)^2)}},$$

$$\epsilon_{rms} = \sqrt{\frac{\sum_{j=1}^{m} (\mathcal{U}(\boldsymbol{\sigma}_j, t) - \mathcal{U}_k(\boldsymbol{\sigma}_j, t))^2}{m}},$$

where $\mathcal{U}(\boldsymbol{\sigma}_j, t)$ and $\mathcal{U}_k(\boldsymbol{\sigma}_j, t)$ denotes the exact and numerical solutions respectively.

5.1. Problem 1

We consider Eq. (1) with $\zeta = \xi = 1$, and $\lambda = 0$ and exact solution $\mathcal{U}(x, y, t) = x^2 + y^2 + t^2$. The results obtained along the path Γ with parameter values in Set 1 are shown in Table 1, and with parameters values in Set 2 are shown in Table 2. The LTCSCM solution of the problem 1 is shown in Fig. 1(a). The errors obtained for $t \in [0, 1]$ are presented in Fig. 1(b). Similarly the errors obtained for various values of M using the parameter Set 1 and Set 2 are depicted in Figs. 2(a) and 2(b) respectively. From all the results presented in Tables and figures very high accuracy is evident.

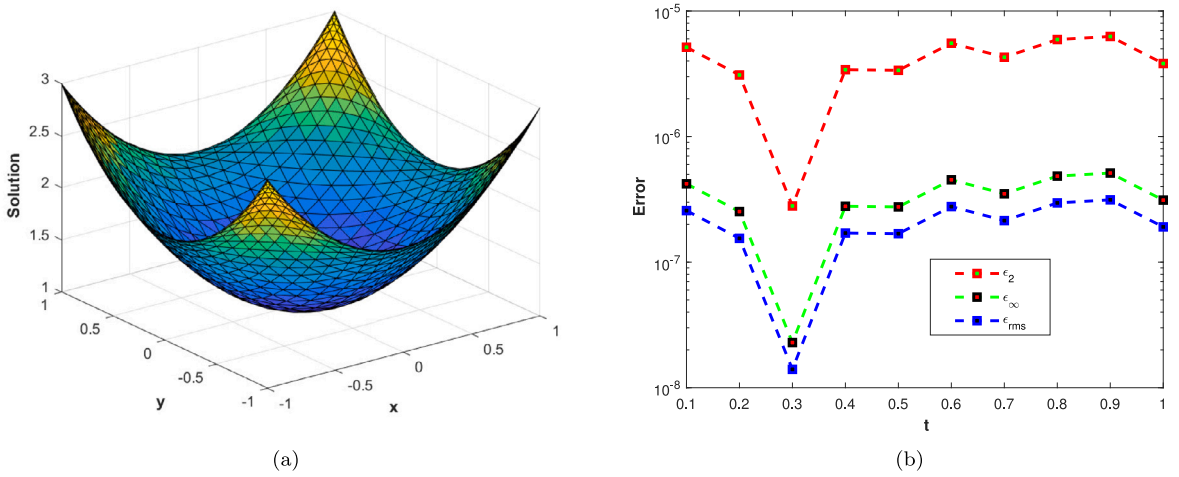

Fig. 1. (a) LTCSCM solution of problem 1 (b) Plots of ϵ_2, ϵ_∞ and ϵ_{rms} for $t \in [0, 1]$ for problem 1 with $M = 90$ *and* $m = 28$.

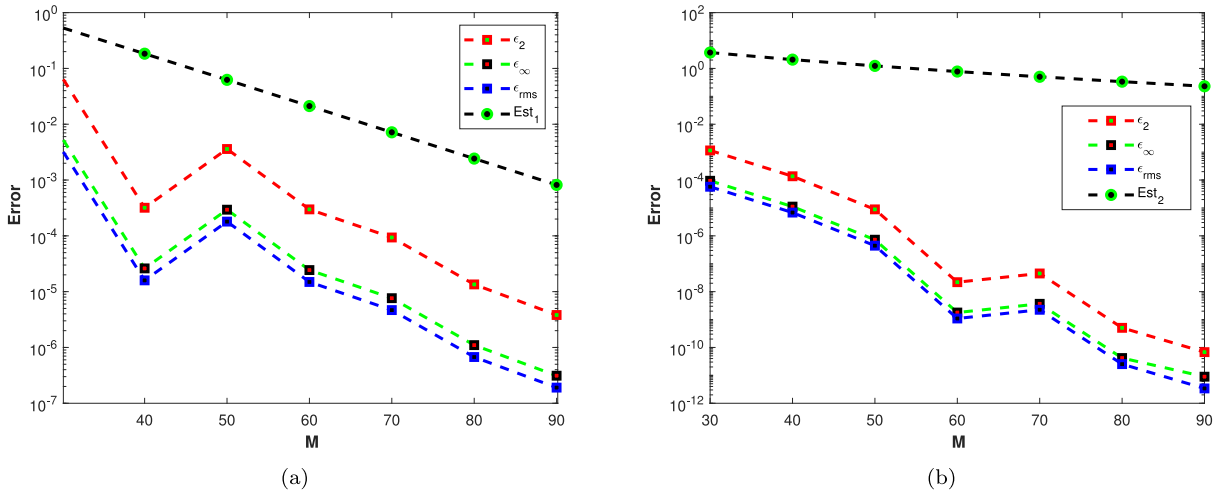

Fig. 2. (a) Plots of ϵ_2, ϵ_∞ and ϵ_{rms} versus M with $m = 30$, $t = 1$ and parameter Set 1. (b) Plots of ϵ_2, ϵ_∞ and ϵ_{rms} versus M with $m = 30$, $t = 1$ and parameter Set 2.

5.2. Problem 2

We consider Eq. (1) with $\zeta = \xi = 1$, and $\lambda = 0$ and exact solution $\mathcal{U}(x, y, t) = x^2 + y^2 + e^{-\pi^2 t^2}$. The results obtained along the path Γ with parameter values in Set 1 are shown in Table 3, and with parameters values in Set 2 are shown in Table 4. The LTCSCM solution of the problem 2 is depicted in Fig. 3(a). The graphs of obtained errors for $t \in [0, 1]$ are displayed in Fig. 3(b). Similarly the errors obtained for numerous values of M using the parameter Set 1 and Set 2 are depicted in Figs. 4(a) and 4(b) respectively. The results demonstrates the efficiency of the numerical scheme.

5.3. Problem 3

We consider Eq. (1) with $\zeta = \xi = 1$, and $\lambda = 0$ and exact solution $\mathcal{U}(x, y, t) = (t^3 + 1)(1 - x^2 - y^2)$. The results obtained along the path Γ with parameter values in Set 1 are shown in Table 5, and with parameters values in Set 2 are shown in Table 6. The LTCSCM solution of the problem 3 is depicted shown in Fig. 5(a). The plots obtained errors for $t \in [0, 1]$ are depicted in Fig. 5(b). Similarly the errors obtained for various values of M using the parameter Set 1 and Set 2 are shown in Figs. 6(a) and 6(b) respectively. We observe that the LTCSCM and analytic solution agrees well.

Table 3
The ϵ_2, ϵ_∞, ϵ_{rms} and Est_1 of the LTCSCM for problem 2.

m	M	ϵ_2	ϵ_∞	ϵ_{rms}	Est_1	C.time (s)
22	90	4.1270×10^{-4}	3.9508×10^{-5}	1.8759×10^{-5}	8.1825×10^{-4}	48.444949
24		4.5022×10^{-4}	3.9535×10^{-5}	1.8759×10^{-5}	8.1825×10^{-4}	73.728131
26		4.8773×10^{-4}	3.9550×10^{-5}	1.8759×10^{-5}	8.1825×10^{-4}	108.188960
28		5.2525×10^{-4}	3.9558×10^{-5}	1.8759×10^{-5}	8.1825×10^{-4}	159.456121
30		5.6277×10^{-4}	3.9561×10^{-5}	1.8759×10^{-5}	8.1825×10^{-4}	231.182424
30	50	8.3521×10^{-3}	4.3940×10^{-4}	2.7840×10^{-4}	6.2465×10^{-2}	67.591168
	60	6.8191×10^{-4}	3.9072×10^{-5}	2.2730×10^{-5}	2.1185×10^{-2}	99.503087
	70	6.6155×10^{-4}	3.9691×10^{-5}	2.2052×10^{-5}	7.1708×10^{-3}	137.163385
	80	5.5418×10^{-4}	3.9544×10^{-5}	1.8473×10^{-5}	2.4236×10^{-3}	179.459988
	90	5.6277×10^{-4}	3.9561×10^{-5}	1.8759×10^{-5}	8.1825×10^{-4}	231.182424

Table 4
The ϵ_2, ϵ_∞, ϵ_{rms} and Est_2 of the LTCSCM for problem 2.

m	M	ϵ_2	ϵ_∞	ϵ_{rms}	Est_2	C.time (s)
22	90	4.1042×10^{-4}	3.9498×10^{-5}	1.8655×10^{-5}	2.2972×10^{-1}	56.294827
24		4.4773×10^{-4}	3.9526×10^{-5}	1.8655×10^{-5}	2.2972×10^{-1}	87.371074
26		4.8504×10^{-4}	3.9543×10^{-5}	1.8655×10^{-5}	2.2972×10^{-1}	125.211449
28		5.2235×10^{-4}	3.9551×10^{-5}	1.8655×10^{-5}	2.2972×10^{-1}	181.093252
30		5.5966×10^{-4}	3.9554×10^{-5}	1.8655×10^{-5}	2.2972×10^{-1}	254.744377
30	50	5.6477×10^{-4}	3.9567×10^{-5}	1.8826×10^{-5}	1.2351×10^{0}	76.767423
	60	5.5967×10^{-4}	3.9554×10^{-5}	1.8656×10^{-5}	7.7317×10^{-1}	111.402392
	70	5.5969×10^{-4}	3.9554×10^{-5}	1.8656×10^{-5}	5.0201×10^{-1}	152.667346
	80	5.5966×10^{-4}	3.9554×10^{-5}	1.8655×10^{-5}	3.3556×10^{-1}	201.996580
	90	5.5966×10^{-4}	3.9554×10^{-5}	1.8655×10^{-5}	2.2972×10^{-1}	259.660631

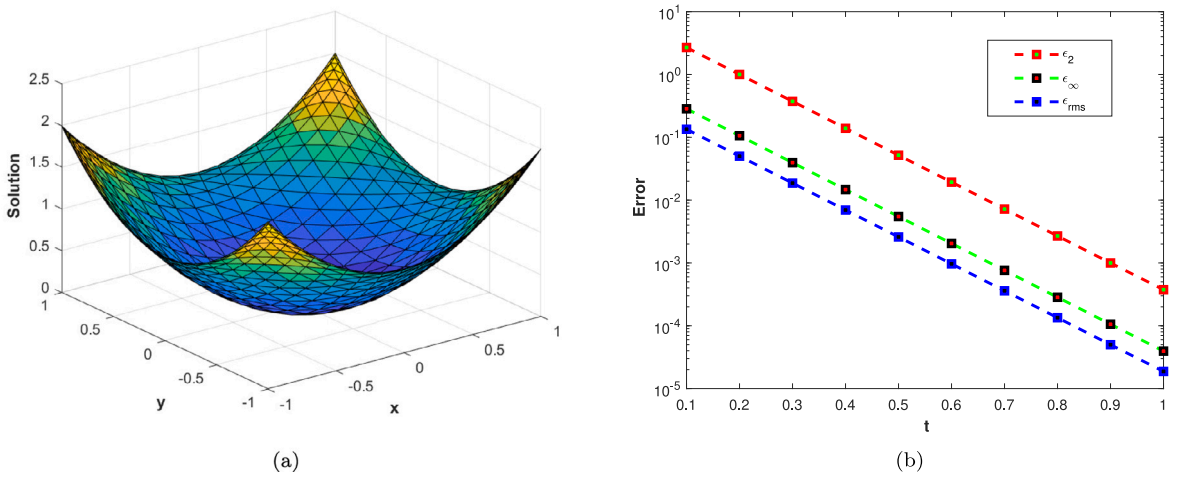

Fig. 3. (a) LTCSCM solution problem 2 (b)Plots of ϵ_2, ϵ_∞ and ϵ_{rms} for $t \in [0, 1]$ for problem 2 with $M = 90$ *and* $m = 28$.

5.4. Problem 4

We consider Eq. (1) with $\zeta = \xi = 1$, and $\lambda = 0$ and exact solution $\mathcal{U}(x, y, t) = \Big(cos(x) + cos(y)\Big)t^4$. The results obtained along the path Γ with parameter values in Set 1 are shown in Table 7, and with parameters values in Set 2 are shown in Table 8. The LTCSCM solution of the problem 4 are shown in Fig. 7(a). The graphs of obtained errors for $t \in [0, 1]$ are shown in Fig. 7(b). Similarly the errors obtained for various values of M using the parameter Set 1 and Set 2 are depicted in Figs. 8(a) and 8(b) respectively. The computational results confirms the efficiency of the method.

5.5. Problem 5

We consider Eq. (1) with $\zeta = \xi = 1$, and $\lambda = 0$ and exact solution $\mathcal{U}(x, y, t) = sin(x + y) + t^2$. The results obtained along the path Γ with parameter values in Set 1 are shown in Table 9, and with parameters values in Set 2 are shown in Table 10. The LTCSCM

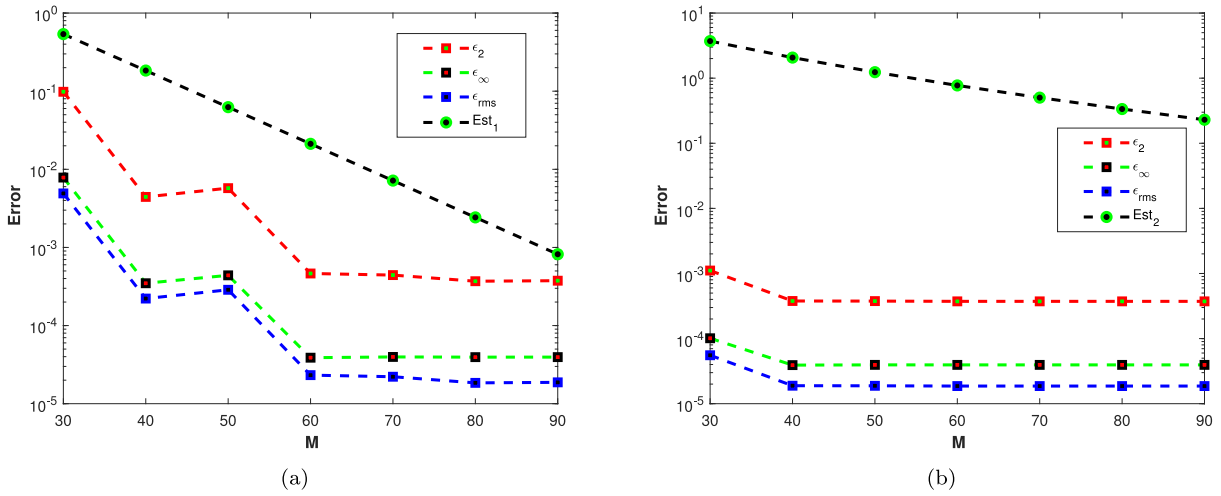

Fig. 4. (a) Plots of ϵ_2, ϵ_∞ and ϵ_{rms} versus M with $m = 30$, $t = 1$ and parameter Set 1. (b) Plots of ϵ_2, ϵ_∞ and ϵ_{rms} versus M with $m = 30$, $t = 1$ and parameter Set 2.

Table 5
The ϵ_2, ϵ_∞, ϵ_{rms} and Est_1 of the LTCSCM for problem 3.

m	M	ϵ_2	ϵ_∞	ϵ_{rms}	Est_1	C.time (s)
22	90	1.8360×10^{-6}	1.5602×10^{-7}	8.3454×10^{-8}	8.1825×10^{-4}	53.762542
24		1.9919×10^{-6}	1.5601×10^{-7}	8.2997×10^{-8}	8.1825×10^{-4}	80.620697
26		2.1476×10^{-6}	1.5601×10^{-7}	8.2601×10^{-8}	8.1825×10^{-4}	113.507853
28		2.3032×10^{-6}	1.5601×10^{-7}	8.2257×10^{-8}	8.1825×10^{-4}	173.250425
30		2.4602×10^{-6}	1.5601×10^{-7}	8.2006×10^{-8}	8.1825×10^{-4}	241.855233
30	50	2.3209×10^{-3}	1.4723×10^{-4}	7.7364×10^{-5}	6.2465×10^{-2}	74.139479
	60	1.9215×10^{-4}	1.2189×10^{-5}	6.4049×10^{-6}	2.1185×10^{-2}	99.603207
	70	6.0247×10^{-5}	3.8218×10^{-6}	2.0082×10^{-6}	7.1708×10^{-3}	137.771173
	80	8.6859×10^{-6}	5.5100×10^{-7}	2.8953×10^{-7}	2.4236×10^{-3}	179.909737
	90	2.4602×10^{-6}	1.5601×10^{-7}	8.2006×10^{-8}	8.1825×10^{-4}	241.855233

Table 6
The ϵ_2, ϵ_∞, ϵ_{rms} and Est_2 of the LTCSCM for problem 3.

m	M	ϵ_2	ϵ_∞	ϵ_{rms}	Est_2	C.time (s)
22	90	3.5466×10^{-11}	5.7705×10^{-12}	1.6121×10^{-12}	2.2972×10^{-1}	53.762542
24		3.7339×10^{-11}	4.0821×10^{-12}	1.5558×10^{-12}	2.2972×10^{-1}	80.620697
26		4.1162×10^{-11}	5.5704×10^{-12}	1.5832×10^{-12}	2.2972×10^{-1}	131.115069
28		5.8645×10^{-11}	3.0211×10^{-12}	2.0945×10^{-12}	2.2972×10^{-1}	173.250425
30		4.7680×10^{-11}	8.9950×10^{-12}	1.5893×10^{-12}	2.2972×10^{-1}	241.855233
30	50	5.7318×10^{-6}	3.6360×10^{-7}	1.9106×10^{-7}	1.2351×10^{0}	74.588554
	60	1.4078×10^{-8}	8.9321×10^{-10}	4.6927×10^{-10}	7.7317×10^{-1}	105.028965
	70	2.8896×10^{-8}	1.8334×10^{-11}	9.6321×10^{-10}	5.0201×10^{-1}	144.471290
	80	3.2763×10^{-10}	2.5309×10^{-11}	1.0921×10^{-11}	3.3556×10^{-1}	191.526822
	90	4.7680×10^{-11}	8.9950×10^{-12}	1.5893×10^{-12}	2.2972×10^{-1}	255.955314

solution of the problem 5 are shown in Fig. 9(a). The graphs of errors obtained for $t \in [0, 1]$ are shown in Fig. 9(b). Similarly plots the errors of the for various values of M using the parameter Set 1 and Set 2 are presented in Fig. 10(a) and Fig. 10(b) respectively.

6. Conclusion

In this article, a very highly accurate method based on LT and CSCM was developed for the numerical treatment of 2-D ADEs. The method uses LT to handle the time derivative avoiding the time stepping technique and CSCM to approximate the spatial derivative with high accuracy. The proposed scheme method does not have stability limits, which is an issue frequently encountered in finite difference time stepping methods, and is nearly accurate in time. These methods require very small time steps for highest level of accuracy. Furthermore, the CSCM makes this approach fascinating and simple to use. This method has the advantages of being straightforward to use and highly accurate numerical method for the solution of PDEs. We can deduce from the numerical and graphical results that the proposed method is more accurate, efficient, and stable.

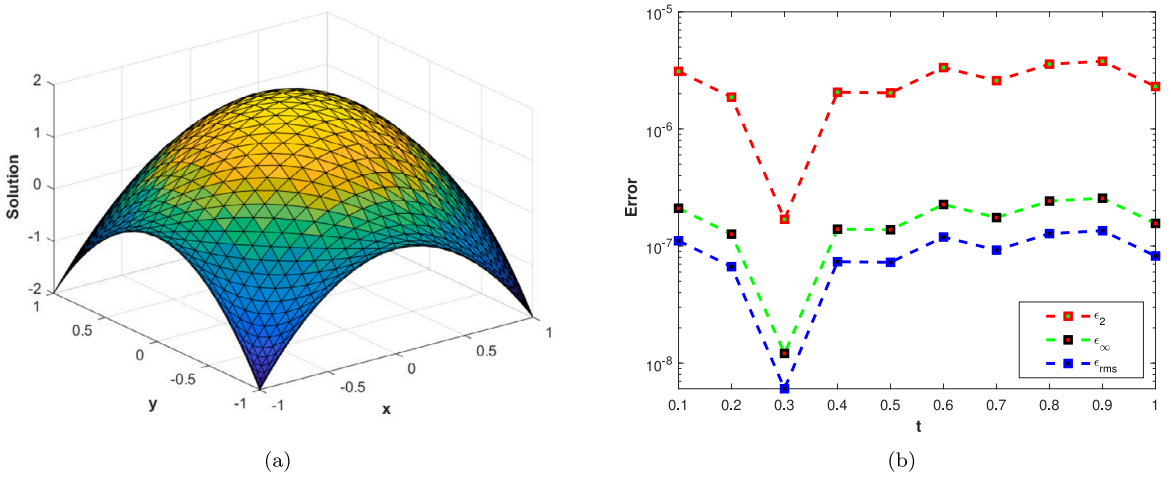

Fig. 5. (a) LTCSCM solution problem 3 (b) Plots of ϵ_2, ϵ_∞ and ϵ_{rms} for $t \in [0, 1]$ for problem 3 with $M = 90$ *and* $m = 28$.

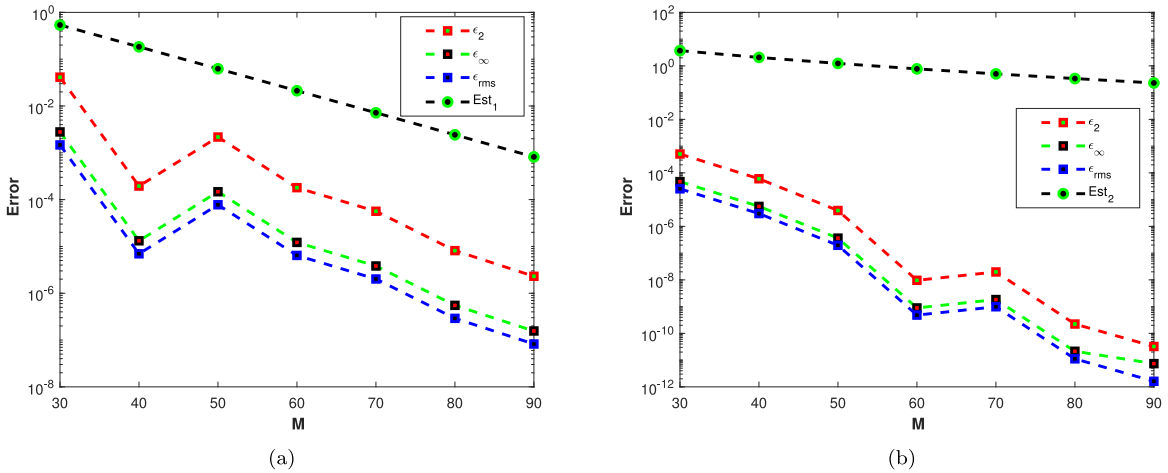

Fig. 6. (a) Plots of ϵ_2, ϵ_∞ and ϵ_{rms} versus M with $m = 30$, $t = 1$ and parameter Set 1. (b) Plots of ϵ_2, ϵ_∞ and ϵ_{rms} versus M with $m = 30$, $t = 1$ and parameter Set 2.

Table 7
The ϵ_2, ϵ_∞, ϵ_{rms} and Est_1 of the LTCSCM for problem 4.

m	M	ϵ_2	ϵ_∞	ϵ_{rms}	Est_1	C.time (s)
22	90	3.1110×10^{-8}	9.7438×10^{-9}	1.4141×10^{-9}	8.1825×10^{-4}	62.363415
24		5.1123×10^{-8}	2.0624×10^{-8}	2.1301×10^{-9}	8.1825×10^{-4}	82.808411
26		6.1553×10^{-8}	2.9023×10^{-8}	2.3674×10^{-9}	8.1825×10^{-4}	135.542622
28		1.0940×10^{-7}	2.0522×10^{-8}	3.9072×10^{-9}	8.1825×10^{-4}	172.642495
30		1.6639×10^{-7}	4.4759×10^{-8}	5.5462×10^{-9}	8.1825×10^{-4}	240.492803
30	50	1.7506×10^{-6}	7.2197×10^{-7}	5.8354×10^{-8}	6.2465×10^{-2}	66.214812
	60	1.0163×10^{-6}	3.9429×10^{-7}	3.3876×10^{-8}	2.1185×10^{-2}	95.898721
	70	5.3041×10^{-7}	1.5862×10^{-7}	1.7680×10^{-8}	7.1708×10^{-3}	134.390339
	80	2.7324×10^{-7}	5.7649×10^{-8}	9.1080×10^{-9}	2.4236×10^{-3}	171.040636
	90	1.6639×10^{-7}	4.4759×10^{-8}	5.5462×10^{-9}	8.1825×10^{-4}	221.736711

Table 8
The ϵ_2, ϵ_∞, ϵ_{rms} and Est_2 of the LTCSCM for problem 4.

m	M	ϵ_2	ϵ_∞	ϵ_{rms}	Est_2	C.time (s)
22	90	2.4727×10^{-11}	5.5755×10^{-11}	1.1240×10^{-12}	2.2972×10^{-1}	54.213764
24		4.0895×10^{-11}	1.3200×10^{-11}	1.7040×10^{-12}	2.2972×10^{-1}	81.326134
26		7.0086×10^{-11}	1.5439×10^{-11}	2.6956×10^{-12}	2.2972×10^{-1}	117.908875
28		9.3381×10^{-11}	2.8318×10^{-11}	3.3350×10^{-12}	2.2972×10^{-1}	174.175306
30		1.3010×10^{-11}	3.7535×10^{-11}	4.3365×10^{-12}	2.2972×10^{-1}	239.389377
30	50	2.0240×10^{-10}	5.3098×10^{-11}	6.7467×10^{-12}	1.2351×10^{0}	75.931907
	60	1.4265×10^{-10}	3.9854×10^{-11}	4.7550×10^{-12}	7.7317×10^{-1}	105.001478
	70	1.3946×10^{-10}	5.4384×10^{-11}	4.6487×10^{-12}	5.0201×10^{-1}	142.130044
	80	1.2675×10^{-10}	3.6433×10^{-11}	4.2251×10^{-12}	3.3556×10^{-1}	186.955650
	90	1.3010×10^{-10}	3.7535×10^{-11}	4.3365×10^{-12}	2.2972×10^{-1}	239.389377

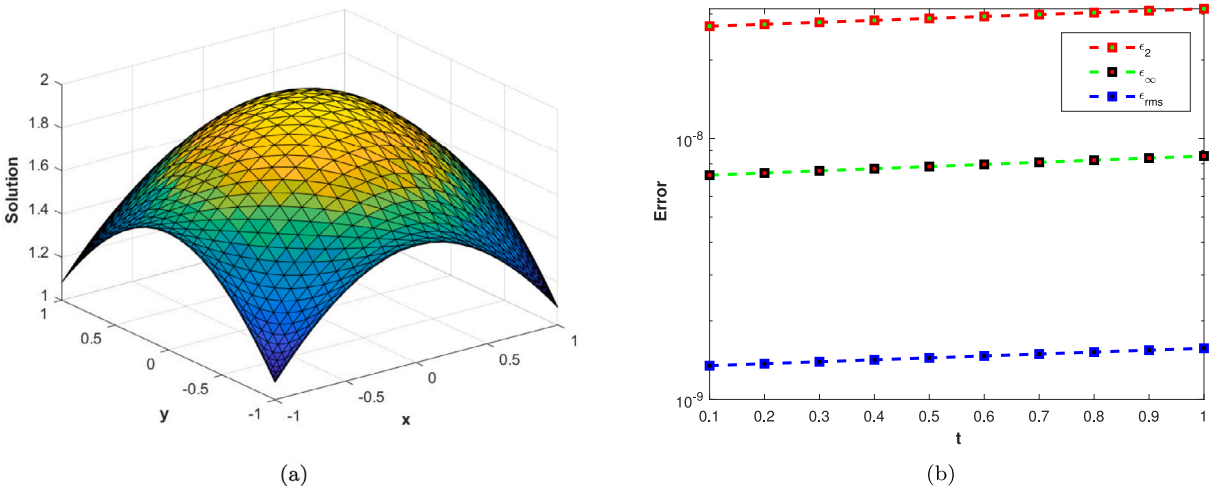

Fig. 7. (a) LTCSCM solution problem 4 (b) Plots of ϵ_2, ϵ_∞ and ϵ_{rms} for $t \in [0, 1]$ for problem 4 with $M = 90$ *and* $m = 28$.

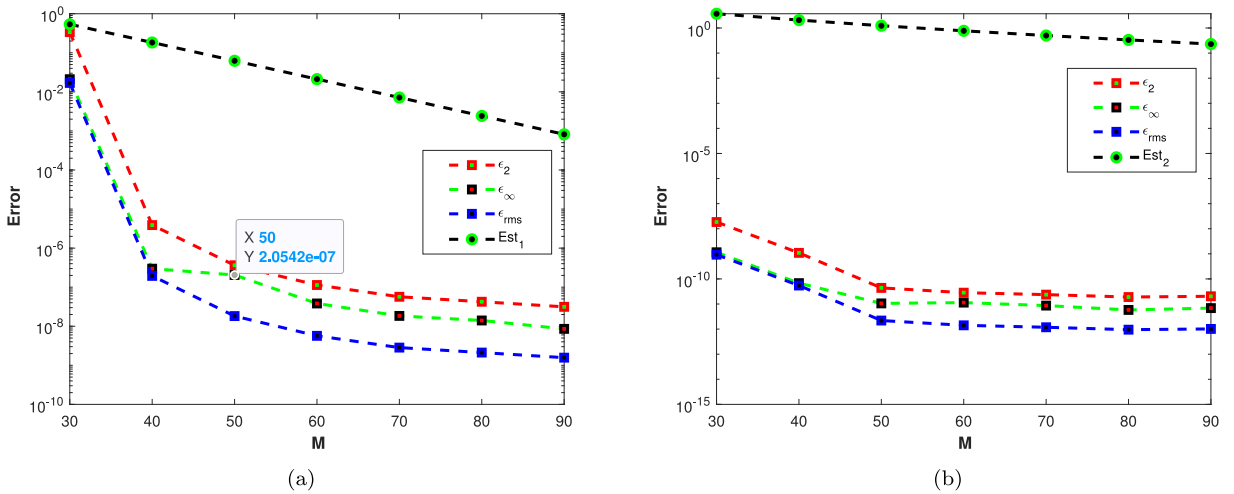

Fig. 8. (a) Plots of ϵ_2, ϵ_∞ and ϵ_{rms} versus M with $m = 30$, $t = 1$ and parameter Set 1. (b) Plots of ϵ_2, ϵ_∞ and ϵ_{rms} versus M with $m = 30$, $t = 1$ and parameter Set 2.

Table 9
The ϵ_2, ϵ_∞, ϵ_{rms} and Est_1 of the LTCSCM for problem 5.

m	M	ϵ_2	ϵ_∞	ϵ_{rms}	Est_1	C.time (s)
22	90	2.4880×10^{-6}	1.5606×10^{-7}	1.1309×10^{-7}	8.1825×10^{-4}	48.027971
24		2.7031×10^{-6}	1.5606×10^{-7}	1.1263×10^{-7}	8.1825×10^{-4}	75.131954
26		2.9182×10^{-6}	1.5606×10^{-7}	1.1224×10^{-7}	8.1825×10^{-4}	108.308410
28		3.1333×10^{-6}	1.5606×10^{-7}	1.1190×10^{-7}	8.1825×10^{-4}	158.029414
30		3.3484×10^{-6}	1.5606×10^{-7}	1.1161×10^{-7}	8.1825×10^{-4}	215.837634
30	50	3.1600×10^{-3}	1.4738×10^{-4}	1.0533×10^{-4}	6.2465×10^{-2}	69.349633
	60	2.6164×10^{-4}	1.2197×10^{-5}	8.7212×10^{-6}	2.1185×10^{-2}	104.468417
	70	8.2024×10^{-5}	3.8237×10^{-6}	2.7341×10^{-6}	7.1708×10^{-3}	132.624142
	80	1.1826×10^{-5}	5.5121×10^{-7}	3.9420×10^{-7}	2.4236×10^{-3}	195.304576
	90	3.3484×10^{-6}	1.5606×10^{-7}	1.1161×10^{-7}	8.1825×10^{-4}	225.264458

Table 10
The ϵ_2, ϵ_∞, ϵ_{rms} and Est_2 of the LTCSCM for problem 5.

m	M	ϵ_2	ϵ_∞	ϵ_{rms}	Est_2	C.time (s)
22	90	4.4188×10^{-11}	3.5993×10^{-12}	2.0085×10^{-12}	2.2972×10^{-1}	55.284701
24		4.9276×10^{-11}	3.7834×10^{-12}	2.0532×10^{-12}	2.2972×10^{-1}	84.404177
26		5.2801×10^{-11}	4.0121×10^{-12}	2.0308×10^{-12}	2.2972×10^{-1}	122.908011
28		5.6345×10^{-11}	6.0949×10^{-12}	2.0123×10^{-12}	2.2972×10^{-1}	181.390191
30		6.1160×10^{-11}	6.4453×10^{-12}	2.0387×10^{-12}	2.2972×10^{-1}	247.254575
30	50	7.8042×10^{-6}	3.6391×10^{-7}	2.6014×10^{-7}	1.2351×10^{0}	75.647948
	60	1.9167×10^{-8}	8.9422×10^{-10}	6.3888×10^{-10}	7.7317×10^{-1}	110.368982
	70	3.9348×10^{-8}	1.8343×10^{-9}	1.3116×10^{-9}	5.0201×10^{-1}	149.329200
	80	4.4383×10^{-10}	2.3038×10^{-11}	1.4794×10^{-11}	3.3556×10^{-1}	195.569956
	90	6.1160×10^{-11}	6.4453×10^{-12}	2.0387×10^{-12}	2.2972×10^{-1}	247.254575

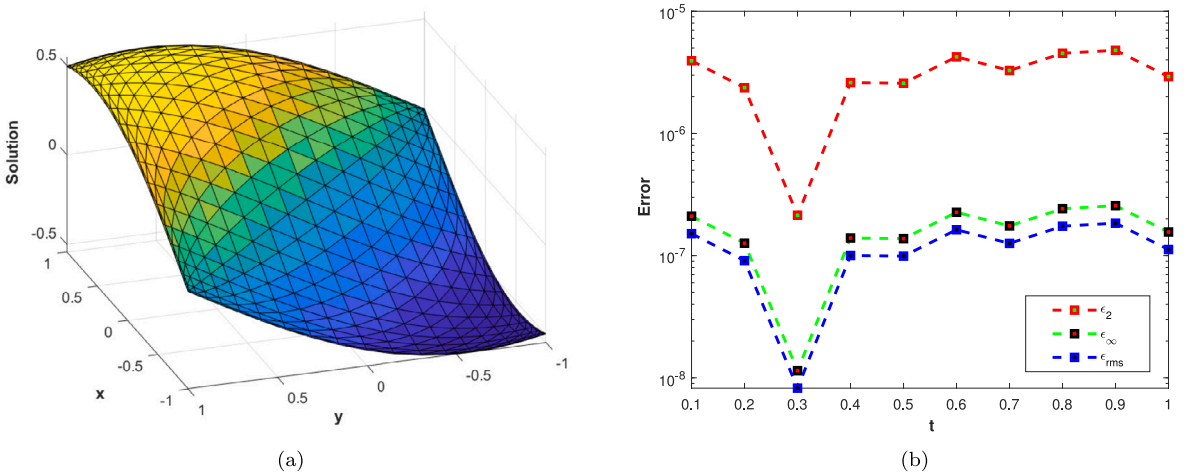

Fig. 9. (a) LTCSCM solution problem 5 (b) Plots of ϵ_2, ϵ_∞ and ϵ_{rms} for $t \in [0, 1]$ for problem 5 with $M = 90$ *and* $m = 28$.

Declaration of competing interest

All the authors contributed in theoretical and computational results and approved the final manuscript. The authors declare that they have no conflict of interests

Data availability

No data was used for the research described in the article.

Acknowledgements

Kamal Shah, and Thabet Abdeljawad are thankful to Prince Sultan University, Saudi Arabia for paying the APC and support through the TAS research lab.

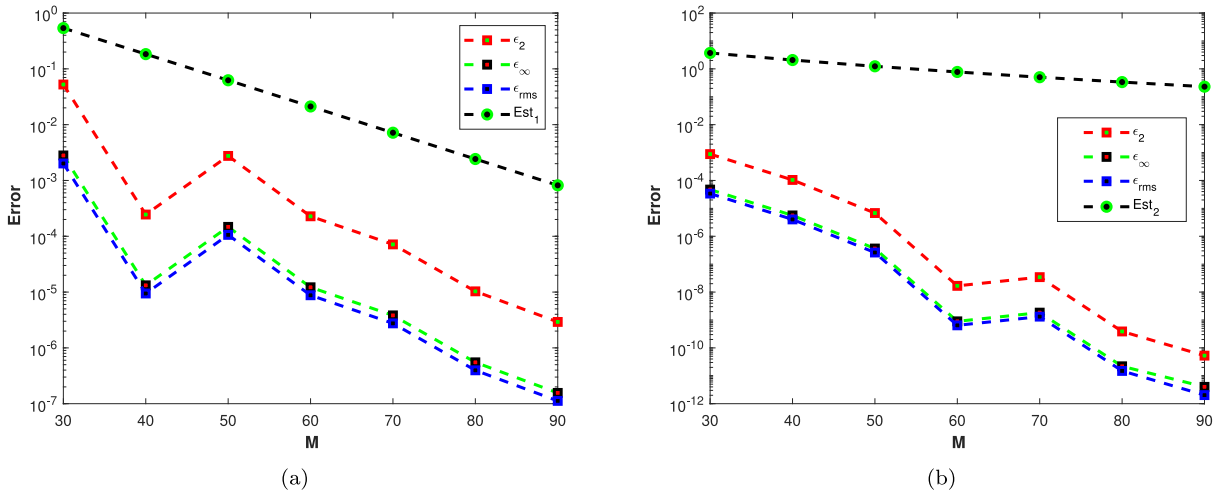

Fig. 10. (a) Plots of ϵ_2, ϵ_∞ and ϵ_{rms} versus M with $m = 30$, $t = 1$ and parameter Set 1. (b) Plots of ϵ_2, ϵ_∞ and ϵ_{rms} versus M with $m = 30$, $t = 1$ and parameter Set 2.

References

[1] Mogre SS, Brown AI, Koslover EF. Getting around the cell: physical transport in the intracellular world. Phys Biol 2020;17(6):061003.
[2] Weaver AT, Mirouze I. On the diffusion equation and its application to isotropic and anisotropic correlation modelling in variational assimilation. Q J R Meteorol Soc 2013;139(670):242–60.
[3] Gokulavani P, Muthtamilselvan M, Abdalla B, Doh DH. Radiation effect of ND–Ni nanocomposite, water-filled multiport cavity with heated baffle. Eur Phys J Spec Top 2021;230:1201–11.
[4] Palaniappan G, Murugan M, Al-Mdallal QM, Abdalla B, Doh DH. Numerical investigation of open cavities with parallel insulated baffles. Int J Heat Technol 2020;38(3).
[5] Nawaz Y, Arif MS, Shatanawi W, Nazeer A. An explicit fourth-order compact numerical scheme for heat transfer of boundary layer flow. Energies 2021;14(12):3396.
[6] Arif MS, Abodayeh K, Nawaz Y. The modified finite element method for heat and mass transfer of unsteady reacting flow with mixed convection. Front Phys 2022;10:952787.
[7] Dehghan M. Weighted finite difference techniques for the one-dimensional advection-diffusion equation. Appl Math Comput 2004;147(2):307–19.
[8] Mittal RC, Jain R. Redefined cubic B-splines collocation method for solving convection–diffusion equations. Appl Math Model 2012;36(11):5555–73.
[9] Parlange JY. Water transport in soils. Annu Rev Fluid Mech 1980;12(1):77–102.
[10] Zlatev Z, Berkowicz R, Prahm LP. Implementation of a variable stepsize variable formula method in the time-integration part of a code for treatment of long-range transport of air pollutants. J Comput Phys 1984;55(2):278–301.
[11] Goh J, Ismail AIM. Cubic B-spline collocation method for one-dimensional heat and advection-diffusion equations. J Appl Math 2012. 2012.
[12] Kumar DK, Kumar N. Analytical solutions of one-dimensional advection-diffusion equation with variable coefficients in a finite domain. J Earth Syst Sci 2009;118:539–49.
[13] Kumar DK, Kumar N. Analytical solutions to one-dimensional advection-diffusion equation with variable coefficients in semi-infinite media. J Hydrol 2010;380:330–7.
[14] Zoppou C, Knight JH. Analytical solution of a spatially variable coefficient advection–diffusion equation in up to three dimensions. Appl Math Model 1999;23(9):667–85.
[15] Jha BK, Adlakha N, Mehta MN. Analytic solution of two-dimensional advection diffusion equation arising in cytosolic calcium concentration distribution. Int Math Forum 2012;7:135–44.
[16] Carr EJ. New semi-analytical solutions for advection–dispersion equations in multilayer porous media. Transp Porous Media 2020;135(1):39–58.
[17] Kojouharov VH, Chen-Charpentier BM. An unconditionally positivity preserving scheme for advection-diffusion reaction equations. Math Comput Modelling 2013;57:1277–85.
[18] Ismail HN, Elbarbary EM, Salem GS. Restrictive Taylor's approximation for solving convection–diffusion equation. Appl Math Comput 2014;147:355–63.
[19] Thongmoon M, McKibbin R. A comparison of some numerical methods for the advection diffusion equation. Res Lett Inf Math Sci 2006;10(49).
[20] Chen W, Hon YC. Numerical investigation on convergence of boundary knot method in the analysis of homogeneous Helmholtz, modified Helmholtz, and convection–diffusion problems. Comput Methods Appl Mech Engrg 2003;192(15):1859–75.
[21] Lin H, Atluri SN. Meshless local Petrov–Galerkin (MLPG) method for convection-diffusion problems. Comput Model Eng Sci 2000;1:45–60.
[22] Gupta MM, Manohar RP, Stephenson JW. A single cell high order scheme for the convection–diffusion equation with variable coefficients. Internat J Numer Methods Fluids 1984;4(7):641–51.
[23] Kamran Shah FA, Aly WHF, Aksoy H, Alotaibi FM, Mahariq I. Numerical inverse Laplace transform methods for advection-diffusion problems. Symmetry 2022;14(12):2544.
[24] Kamran. Ahmadian A, Salahshour S, Salimi M. A robust numerical approximation of advection diffusion equations with nonsingular kernel derivative. Phys Scr 2021;96(12):124015.
[25] Nazir T, Abbas M, Ismail AIM, Majid AA, Rashid A. The numerical solution of advection-diffusion problems using new cubic trigonometric B-splines approach. Appl Math Model 2016;40(7–8):4586–611.
[26] Buzbee BL, Golub GH, Nielson CW. On direct methods for solving Poisson's equations. SIAM J Numer Anal 1970;7(4):627–56.
[27] Clenshaw CW, Curtis AR. A method for numerical integration on an automatic computer. Numer Math 1960;2:197–205.
[28] D. Gottlieb, Orszag SA. Numerical analysis of spectral methods: theory and applications. SIAM; 1977.
[29] D. Koslo, Tal-Ezer H. A modified Chebyshev pseudospectral method with an time step restriction. J Comput Phys 1993;104:457–69.

[30] Trefethen L, N. Spectral methods in matlab. Philadelphia: SIAM; 2000.
[31] Carpenter MH, Gottlieb D. Spectral methods on arbitrary grids. J Comput Phys 1996;129:74–86.
[32] Weideman JAC. Spectral methods based on nonclassical orthogonal polynomials. Int Ser Numer Math 1999;131:238–51.
[33] Mofid A, Peyrett R. Stability of the chevshev collocation approximation to the advection-diffusion equation. Comput & Fluids 1993;22(4–5):453–65.
[34] Elghaoui M, Pasquetti R. A spectral embedding method applied to the advection-diffusion equation. J Comput Phys 1996;125:464–76.
[35] Reddy SC. Trefethen LN. Pseudospectra and the convection–diffusion operator. SIAM J Appl Math 1994;54:1634–49.
[36] Gottlieb D, Lustman L. The spectrum of the Chebyshev collocation operator for the heat equation. SIAM J Numer Anal 1983;20:909–21.
[37] A. B. Orovio AB, Garcia VMP, Fenton FH. Spectral methods for partial differential equations in irregular domains: The spectral smoothed boundary method. SIAM J Sci Comput 2006;28(3):886–900.
[38] Davies AJ, Crann D, Mushtaq J. A parallel Laplace transform method for diffusion problems with discontinuous boundary conditions. WIT Trans Inf Commun Technol 2000;23.
[39] Fu ZJ, Chen W, Yang HT. Boundary particle method for Laplace transformed time fractional diffusion equations. J Comput Phys 2013;235:52–66.
[40] Crump KS. Numerical inversion of Laplace transforms using a Fourier series approximation. J ACM 1976;23(1):89–96.
[41] F.R. Hoog De, Knight JH, Stokes AN. An improved method for numerical inversion of Laplace transforms. SIAM J Sci Stat Comput 1982;3(3):357–66.
[42] Weeks WT. Numerical inversion of Laplace transforms using Laguerre functions. J ACM 1966;13(3):419–29.
[43] Kamran Khan SU, Haque S, Mlaiki N. On the approximation of fractional-order differential equations using Laplace transform and weeks method. Symmetry 2023;15(6):1214.
[44] McLean W, Thomée V. Numerical solution via Laplace transforms of a fractional order evolution equation. J Integr Equations Appl 2010;5:7–94.
[45] Kamran. Ali G, Gómez-Aguilar JF. Approximation of partial integro differential equations with a weakly singular kernel using local meshless method. Alex Eng J 2020;59(4):2091–100.
[46] Baltensperger R, Trummer MR. Spectral differencing with a twist. SIAM J Sci Comput 2003;24(5):1465–87.
[47] Welfert BD. Generation of pseudospectral differentiation matrices I. SIAM J Numer Anal 1997;34(4):1640–57.
[48] Börm S, Grasedyck L, Hackbusch W. Introduction to hierarchical matrices with applications. Eng Anal Bound Elem 2003;27(5):405–22.
[49] Talbot A. The accurate numerical inversion of Laplace transforms. IMA J Appl Math 1979;23(1):97–120.
[50] Martensen E. Zur numerischen auswertung uneigentlicher integrale. ZAMM - J Appl Math Mech 1968;48:T83–5.
[51] Weideman J, Trefethen L. Parabolic and hyperbolic contours for computing the bromwich integral. Math Comp 2007;76(259):1341–56.